ACS Energy LETTERS

http://pubs.acs.org/journal/aelccp

Polythiocyanogen as Cathode Materials for High Temperature All-Solid-State Lithium–Sulfur Batteries

Shen Wang,[‖] Jianbin Zhou,[‖] Shijie Feng, Maansi Patel, Bingyu Lu, Weikang Li, Charles Soulen, Jiaqi Feng, Ying Shirley Meng, and Ping Liu*

Cite This: *ACS Energy Lett.* 2023, 8, 2699–2706

Read Online

ACCESS | Metrics & More | Article Recommendations | Supporting Information

ABSTRACT: **Solid-state lithium batteries are uniquely suited for operation at elevated to even high temperatures (>100 °C). Under these conditions, however, oxide cathode materials are unstable with high-conductivity sulfide-based electrolytes while elemental sulfur suffers from poor utilization due to its insulating nature. Here, we developed an ionic liquid mediated synthesis procedure for polythiocynogen (poly-SCN) and applied it as a sulfur-rich cathode. The material, with uniform, submicrometer particle size and *a* > 55 wt % sulfur loading, exhibits good thermal stability of over 200 °C. A specific capacity of over 800 mAh g^{-1} at 100 °C is realized when poly-SCN is used as a cathode in an all-solid-state battery (ASSB). Mechanistic studies show that during discharge, both C−S and S−S bonds in poly-SCN are cleaved along with the formation of Li_2S. During charge, the re-formation of poly-SCN structure is observed. The scalable synthesis procedure, high thermal stability, high sulfur loading, and high capacity make poly-SCN a promising candidate for high temperature solid state batteries.**

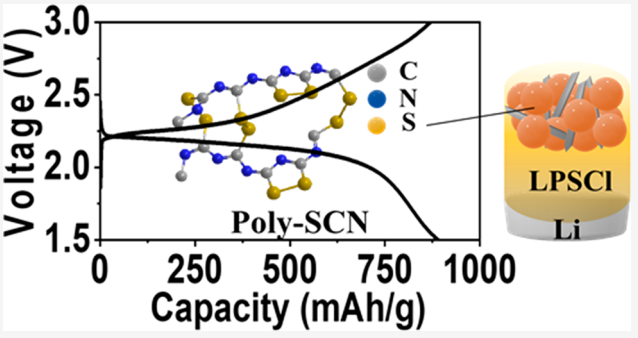

Rechargeable batteries operating at elevated temperatures are important for oil exploration, aerospace engineering, and automotive electronics, among others.[1,2] These operating temperatures, often in excess of 100 °C, pose challenges for liquid-electrolyte batteries due to their volatility and flammable nature.[3] Solid state batteries are ideally suited for elevated temperature operation due to their lack of flammability and the potential of using lithium metal anode which leads to high energy density. Inorganic oxides such as $Li_7La_3Zr_2O_{12}$ (LLZO) have good ionic conductivity and thermal stability with lithium metal[4,5] but are difficult to process and suffer from poor interface with lithium.[6] In contrast, sulfide electrolytes such as Li_3PS_4 (LPS) or Li_6PS_5Cl (LPSCl) have high ionic conductivity and are more ductile, which greatly facilitates processing and device integration.[7]

A major challenge for sulfide electrolytes is their instability at the cathode/electrolyte interface: when applying high voltage transition metal oxides cathode such as $LiCoO_2$ (LCO), $LiNi_xMn_yCo_{(1-x-y)}O_2$ (NMC), or $LiNi_xCo_yAl_{(1-x-y)}O_2$ (NCA), the irreversible cobalt−phosphor cation exchange takes place during charging.[8,9] In contrast, sulfur cathode, with a 1675 mAh g^{-1} theoretical capacity and natural abundance, is ideally suited to match with sulfide electrolytes.[10,11] Unlike in liquid-electrolyte Li−S batteries, ASSBs do not suffer from the well-known "shuttle" phenomenon induced by the dissolution of polysulfides.[12−14] However, the insulating nature of elemental sulfur (~10^{-24} S cm^{-1} conductivity) limits its application in the ASSBs.[15] Multiple mitigation measures have been investigated, including doping,[16,17] nanoconfinement,[18,19] and using sulfur-rich polymers.[20−22] In the polymers, sulfur atoms are bonded with conductive polymeric backbones. The kinetic performance of sulfur is enhanced since it is effectively dispersed as atoms in a polymer matrix.

Polythiocyanogen (poly-SCN)[23−27] has a stoichiometry of $(CNS)_x$ (55 wt % sulfur). Its main chain is a −C═N− conjugated structure. If fully utilized, the material has a theoretical capacity of 926 mAh g^{-1}. Moreover, poly-SCN is a stable photocatalyst under extended light exposure, indicating its promising thermal stability.[23] These properties suggest poly-SCN might be a suitable candidate as a cathode material for high

Received: March 28, 2023
Accepted: May 22, 2023

https://doi.org/10.1021/acsenergylett.3c00659
ACS Energy Lett. 2023, 8, 2699−2706

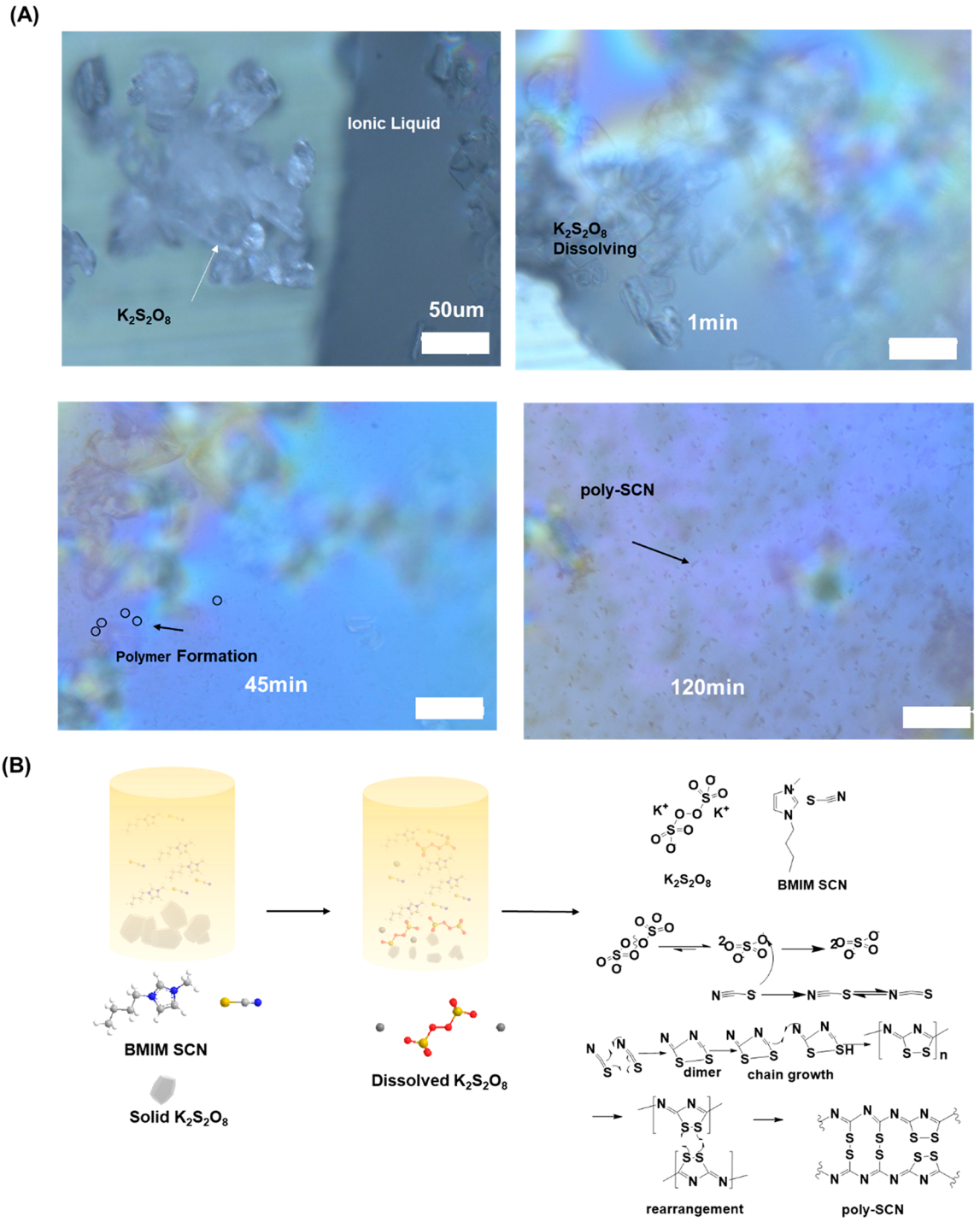

Figure 1. Synthesis procedure for polythiocyanogen (poly-SCN) by a solid−liquid reaction: (A) optical images for ionic precursor (BMIM SCN) reacting with $K_2S_2O_8$ over time to form poly-SCN; (B) proposed poly-SCN reaction mechanism.

temperature ASSBs. There have been several reported methods for synthesizing poly-SCN. In general, a SCN^- precursor (NH_4SCN or KSCN) can be oxidized by H_2SO_4 or Cl_2 to form poly-SCN. These synthesis procedures require either toxic reagents, strong acids, or multiple reaction steps with low yields.[25,27] Alternatively, poly-SCN can be synthesized using a mechanochemical process: KSCN and $K_2S_2O_8$ are hand ground in a mortar and pestle for hours when the SCN^- is polymerized to form poly-SCN.[28] Other mechanical synthesis methods such as ball milling do not work: the heat released during milling can decompose the reaction intermediates, thus yielding products with low sulfur contents (Figure S1A). Finally, poly-SCN has been shown to be a very poor battery material. In liquid electrolytes, the material delivers a reversible capacity of less than 100 mAh g^{-1} from 0.2 to 2 V and the charge storage mechanism remains unknown.[27]

In this study, we report the synthesis of poly-SCN with a solid−liquid reaction (SLR) that can be performed at room temperature in ambient air. The mild reaction condition prevents the thermally induced decomposition and results in high sulfur loading. Moreover, poly-SCN synthesized with this method has more uniform particle size distribution than the one

https://doi.org/10.1021/acsenergylett.3c00659
ACS Energy Lett. 2023, 8, 2699−2706

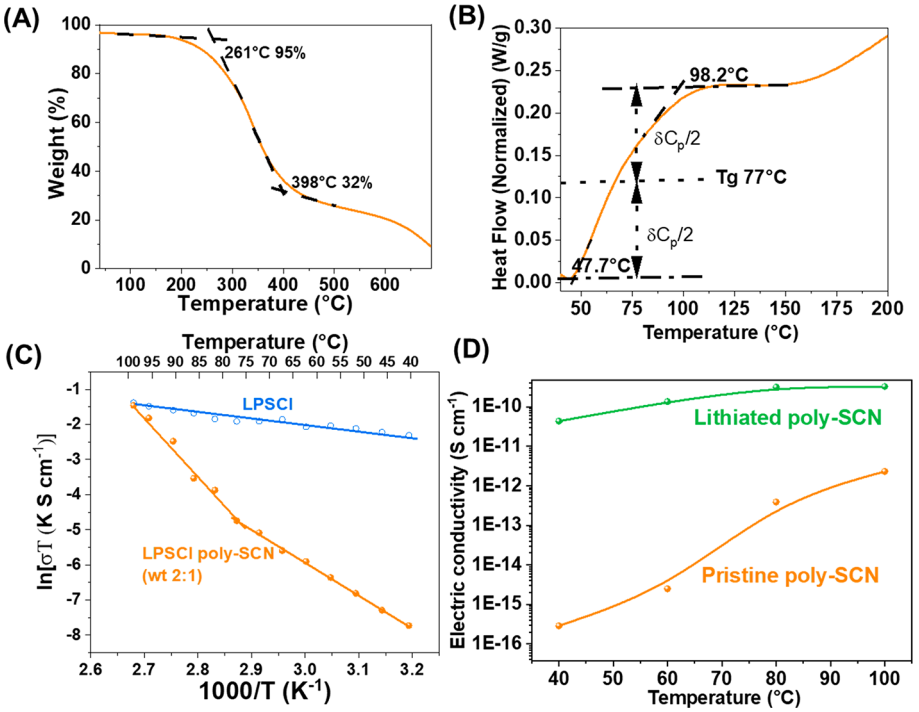

Figure 2. Temperature-dependent properties of poly-SCN: (A) thermogravimetric analysis (TGA) and (B) differential scanning calorimetry (DSC) profiles; (C) Arrhenius plots for LPSCl and LPSCl/poly-SCN (weight ratio 2:1) and (D) electrical conductivity of poly-SCN before and after lithiation.

obtained by mechanical synthesis. When applied as a cathode material in an ASSB operating at 100 °C, poly-SCN delivers a reversible capacity of over 800 mAh g^{-1}, significantly outperforming elemental sulfur. Mechanistic studies reveal that poly-SCN undergoes a solid−solid reaction rather than a solid−liquid−solid reaction experienced by elemental sulfur when operating at these temperatures. Poly-SCN synthesized by the SLR process represents a promising candidate for ASSBs designed for elevated temperature applications.

The SLR synthesis procedure is shown in Figure 1. The liquid precursor 1-butyl-3-methylimidazolium thiocyanate (BMIM SCN) is mixed with the solid oxidizer potassium persulfate ($K_2S_2O_8$). After 2 h, the mixtures are solidified, and the color for the mixtures turns from white into brick red (Figure S1B). The reaction progress over 2 h is recorded under a microscope (Supporting Information Video S1). Images at different points of the video are shown in Figure 1A. Potassium persulfate is first dissolved by the ionic liquid. Once its concentration reaches a critical value at a time stamp of 45 min, the polymerization reaction occurs, forming small yellow particles. The reaction is also tracked with *in situ* Fourier-transform infrared spectroscopy (FTIR) (Figure S1C): in the first 45 min, there is no change. After 45 min, a peak at 1120 cm^{-1} grows, which is attributed to the formation of C═N bonds as a part of the poly-SCN's −C═N− backbone. In the meantime, the imidazolium cation, identified by the peak at 1160 cm^{-1}, remains inert throughout the synthesis process. However, the heightened local concentration of the dissolved $S_2O_8^{2-}$ and poly-SCN can diminish its signal contribution, resulting in a decrease in peak intensity. There are no apparent spectra change after 75 min, suggesting the reaction is self-terminated. Based on these observations, a reaction mechanism for the poly-SCN formation is proposed in Figure 1B: $K_2S_2O_8$ is first dissolved by the precursor BMIM SCN and then starts to oxidize the SCN anion. During the reaction, the bridging O−O bond in $S_2O_8^{2-}$ is cleaved to generate $SO_4^{-\bullet}$ radical anion. This radical anion initiates the SCN^- polymerization and forms SO_4^{2-} in the meantime.[28] Compared to other synthesis approaches, the SLR is performed in the ambient air at room temperature. The yield of poly-SCN based on BMIM SCN is 94%.

Poly-SCN thus obtained has a similar composition as that synthesized by the mechanical hand grinding (HG) method: with an *S*:*N* atomic ratio of 1.2:1 estimated from the X-ray photoelectron spectroscopy (XPS, Figure S1A). However, the mechanical method requires continuous hand grinding of the precursors for 3 h, a method that is not scalable. Attempts of using the ball milling method result in an *S*:*N* ratio of 0.27:1, likely due to the thermal-induced thiocyanate oxidation (Figure S1A).[29] Therefore, we have developed a much more scalable and controllable synthesis process for poly-SCN. The elemental analysis results for SLR poly-SCN are displayed in Table S1; the C:N:S stoichiometry for SLR poly-SCN is close to 1:1:1.

We then characterized the morphology and structure of the poly-SCN synthesized by SLR (SLR poly-SCN); the detailed discussion is included in the Supporting Information "Structure and Properties of SLR poly-SCN" section, and related figures are Figures S2, S3, and S4. In general, the SLR poly-SCN has a conjugated −C═N− structure with −S−S− and −C−S− functional groups. Moreover, compared to the poly-SCN synthesized by hand grinding (HG poly-SCN), the SLR poly-SCN has a much more uniform size distribution.

The thermal properties are evaluated to assess the potential of poly-SCN as a cathode material for high-temperature ASSBs. Thermogravimetric analysis (TGA) (Figure 2A) shows that the polymer starts to decompose at 261 °C, indicating that the material is more stable than elemental sulfur which starts to vaporize at 150 °C.[30] Differential scanning calorimetry (DSC, Figure 2B) results show that there is no exothermic or

https://doi.org/10.1021/acsenergylett.3c00659
ACS Energy Lett. 2023, 8, 2699−2706

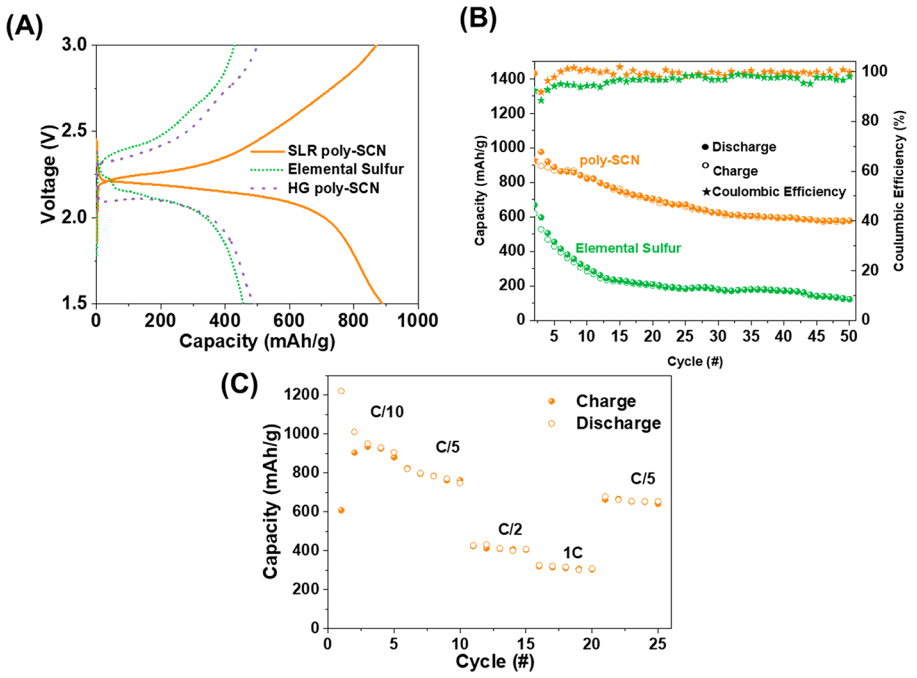

Figure 3. Performance of poly-SCN (synthesized by SLR) as a cathode in solid-state batteries at 100 °C: (A) discharge/charge profiles at the 5th cycle C/5 as compared to those of elemental sulfur and poly-SCN by mechanical synthesis (hand grinding); (B) cycling stability at C/5 as compared to those of elemental sulfur; (C) rate performance.

endothermic peak observed from room temperature to 200 °C. Only a transition from the glassy to rubbery state occurs as the specific heat capacity changes from a temperature of 47.7 to 98.2 °C. Furthermore, the glass transition temperature T_g (at $\delta C_p/2$) for poly-SCN is 77 °C.

Poly-SCN is then blended with an argyrodite-type solid electrolyte Li_6PS_5Cl (LPSCl) to form a composite at a 2:1 weight ratio, the same composition as in an ASSB to be evaluated later. Figure 2C shows the Arrhenius plot for the composite; the results for the pure LPSCl are also included for comparison. There is a slope change for the composite at 77 °C, while there is no slope change in the plot for LPSCl. Therefore, the slope change for the composite is attributed to the behavior of poly-SCN. At 100 °C, the ionic conductivity of the poly-SCN-LPSCl composite (2:1 weight ratio) is slightly reduced from that of pure LPSCl. It indicates the rubbery state poly-SCN at this weight ratio does not greatly impede the ion transport between particles of LPSCl. Additionally, the ionic conductivity of the LPSCl and poly-SCN mixture was measured at various weight ratios at the same temperature (Figure S5). The ion conductivity scales with the amount of LPSCl, again indicating that poly-SCN does not impede ion transport.

The electronic conductivities of poly-SCN before and after lithiation at different temperatures are tested as well, as shown in Figure 2D. Here the lithiated poly-SCN is prepared from pristine poly-SCN reacting with butyllithium. There is a 3 orders of magnitude increase when the temperature increases from 40 to 100 °C, further suggesting that the polymer is more favorable to be operated at elevated temperatures. The primary factor contributing to the low conductivity of poly-SCN at room temperature can be attributed to its limited degree of polymerization, which is determined to be 18 based on mass spectrometry analysis (Figure S3D). Consequently, the material exhibits a wide band gap, as confirmed by ultraviolet photoelectron spectroscopy (UPS, Figure S6), which shows a valence band maximum for poly-SCN exceeding 5 eV relative to the Fermi level. These measurements collectively indicate that it is crucial to operate poly-SCN in its rubbery state at elevated temperatures (>77 °C) when it acquires appreciable conductivity, rendering it well-suited for high-temperature battery applications.

Poly-SCN is then employed to construct ASSBs with LPSCl as the electrolyte and lithium metal as the anode. A carbon interlayer is introduced to limit the side-reaction at the anode/electrolyte interface.[31] In the cathode, LPSCl (ionic conductor) and carbon fiber (electronic conductor) are mixed with poly-SCN. Cryo-FIB-SEM image in Figure S7A shows that the cathode is dense and uniform with a thickness of ~20 μm. EDX image in Figure S7B shows that all components are uniformly distributed in the cathode. There is a clear boundary between the cathode and electrolyte: The N signal from poly-SCN is enriched at the cathode side while invisible in the electrolyte layer.

The ASSBs are tested at 100 °C where poly-SCN has shown high electronic and ionic conductivities. After the first several cycles to form a relative stable cathode−electrolyte interface (Figure S8A), the material shows a reversible capacity of 885 mAh g^{-1} at a rate of C/5 (Figure 3A,B), close to the theoretical capacity of 924 mAh g^{-1}. Further, poly-SCN has a discharge plateau at 2.2 V, much higher than commonly observed in sulfurized polymers.[21] Compared to elemental sulfur, the significant advantage of SLR material persists even after extended cycling, when the elemental sulfur electrode degrades rapidly (Figure 3B). Its rate capability is also good, with capacities of 450 mAh g^{-1} at C/2 and 400 mAh g^{-1} at 1C, respectively (Figures 3C and S8B). At a rate of C/5, poly-SCN significantly outperforms elemental sulfur, which delivers a capacity of 450 mAh g^{-1} (Figure 3A). Likewise, the SLR poly-SCN also outperforms HG poly-SCN, which delivers a capacity of 480 mAh g^{-1}. We attribute this performance difference to

https://doi.org/10.1021/acsenergylett.3c00659
ACS Energy Lett. 2023, 8, 2699−2706

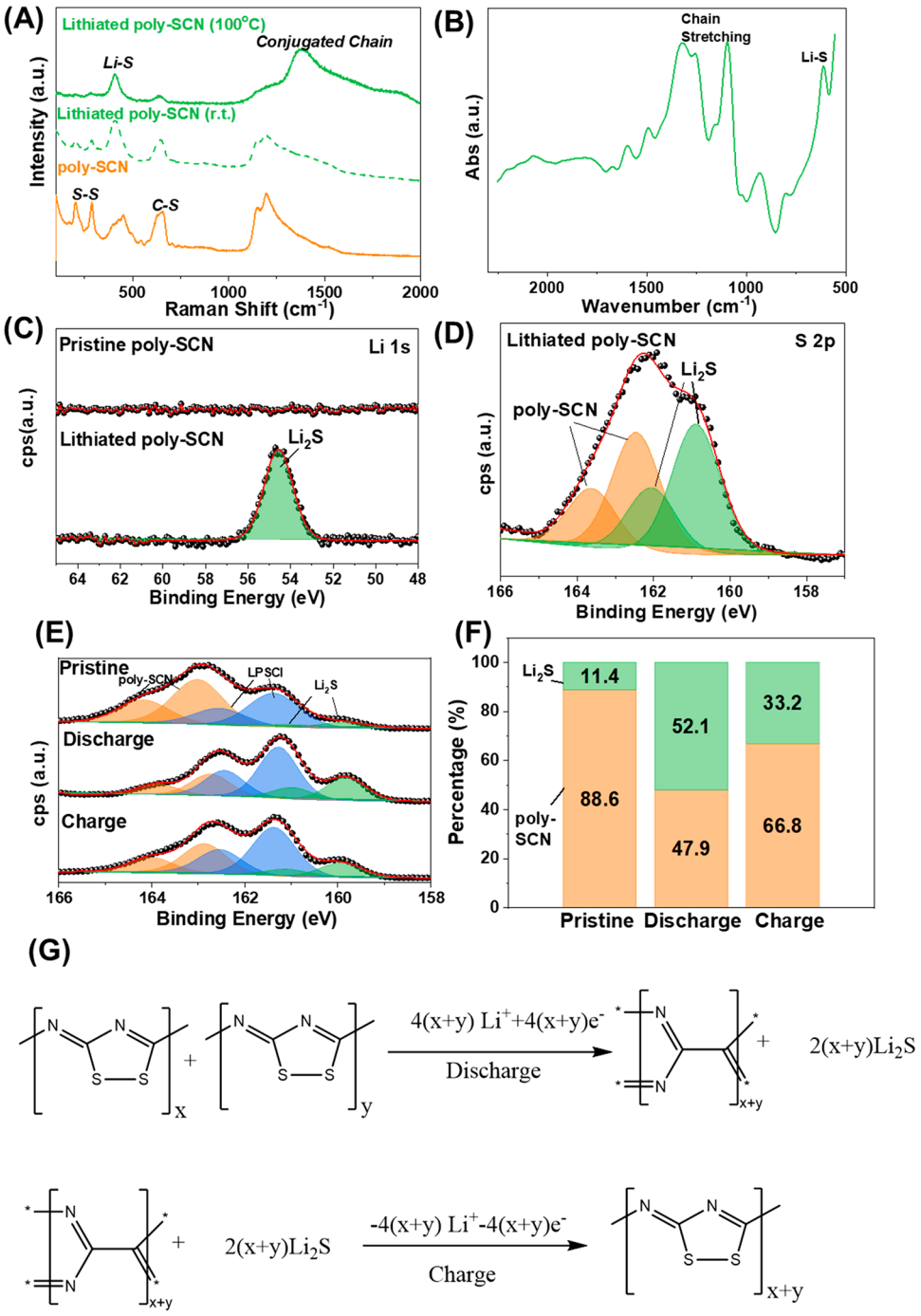

Figure 4. Reaction mechanism during the lithiation/delithiation of poly-SCN: (A) Raman spectra of poly-SCN before and after chemical lithiation; (B) FTIR difference spectra between lithiated poly-SCN and pristine poly-SCN; (C) Li 1s and (D) S 2p XPS spectra for lithiated poly-SCN; (E) S 2p XPS analysis of poly-SCN electrode, extracted from batteries at pristine, charged, and discharged status; (F) composition ratio derived from (E); (G) proposed discharge/charge mechanism for poly-SCN.

their morphological differences: the HG poly-SCN features large particle sizes with broad size distributions than SLR poly-SCN (Figure S2A). Moreover, a temperature-dependent capacity change is observed in the poly-SCN ASSB (Figure S8C): These is almost no capacity once the ASSB was operated below 80 °C which agrees with the previous observation that the rubbery state is crucial for poly-SCN to maintains high electronic and ionic conductivity.

We then studied the working mechanism of poly-SCN in ASSB. As shown in Figure 3A, both SLR and HG poly-SCN show a single voltage plateau during discharge, indicating that the material goes through a solid-phase conversion reaction.[32] This contrasts with elemental sulfur, which exhibits two voltage plateaus. Sulfur discharging at 100 °C appears to follow a "solid−liquid−solid" working mechanism: the plateau at 2.3 V is associated with the transition from Li_2S_8 to Li_2S_6, while the one at 2.1 V is the transition from Li_2S_4 to Li_2S.[10,32] This two-step process takes place even though sulfur is being discharged in the absence of a liquid electrolyte which dissolves the polysulfide

https://doi.org/10.1021/acsenergylett.3c00659
ACS Energy Lett. 2023, 8, 2699−2706

intermediate. The single-phase process might be a result of the limited length of S−S chains in poly-SCN.

To exclude the interference of other cathode components (conductive carbon and LPSCl), we conduct a chemical lithiation of poly-SCN to simulate the discharge product(s). Raman spectra in Figure 4A show a decrease in intensity of the C−S and S−S peaks after chemical lithiation at room temperature. A new peak emerges at 406 cm^{-1}, which is attributed to the formation of Li_2S (Figure S9A). For the lithiated poly-SCN prepared at 100 °C, the C−S and S−S peaks are virtually absent and the Li_2S peak is again observed. Moreover, a broad peak from 1200 to 1600 cm^{-1} associated with the −C═N− conjugated structure is observed. These observations indicate that both C−S and S−S bonds in poly-SCN are cleaved during lithiation, while Li_2S is formed. In the meantime, the degree of −C═N− conjugation increases upon lithiation. Higher temperature facilitates the lithiation reaction, promoting the complete cleavage of C−S and S−S bonds and extending the −C═N− conjugated structure.

The FTIR spectra of poly-SCN before and after chemical lithiation appear to be similar (Figure S9B). However, when taking a difference between them (Figure 4B), we uncover that there is a series of positive −C═N− chain stretching signals in the range of 1000−1500 cm^{-1}. This observation agrees with the conclusion of the growth of the −C═N− chain. Another positive signal is observed at 650 cm^{-1}.[33] This peak is attributed to the $(Li_2S)_1$ cluster, which indicates Li_2S is dispersed in the polymer matrix as a monomer. The formation of Li_2S is also confirmed by XPS shown in Figure 4C,D, with the Li 1s at 54.5 eV and S 2p at 160.5 eV, consistent with Li^+ and S^{2-}, respectively. The survey spectra are shown in Figure S9C. The Li 1s and S 2p positions also demonstrate the lithiation product for poly-SCN is Li_2S.

The mechanism for poly-SCN transformation during charging is studied by post-mortem analysis of the composite cathode harvested from the ASSB by XPS. The S 2p spectra are shown in Figure 4E. In the pristine cathode, the P−S bond (LPSCl) at 161 eV and poly-SCN at 163.1 eV are observed (representing 88.6% of total amount). In the meantime, a small amount of Li_2S (11.4%) is observed, likely due to the moisture induced decomposition of LPSCl.[34] After discharge, the amount of poly-SCN decreases to 47.9% while the amount of Li_2S increases to 52.1%. The formation of Li_2S during discharge agrees with earlier discussion. Furthermore, Figure S10 illustrates the C 1s and N 1s spectra. The C 1s spectra reveal no significant changes, likely due to the high proportion of conductive carbon present. Similarly, the N 1s spectrum exhibits minimal changes in peak characteristics. Considering that poly-SCN is the sole nitrogen-containing component in the cathode, the N 1s results suggest the inert behavior of nitrogen within poly-SCN during battery cycling.

The component ratio of poly-SCN and Li_2S (ionic conductor LPSCl is excluded) derived from the XPS analysis is shown in Figure 4F. After charge, the amount of Li_2S decreases to 33.2% while the amount of poly-SCN increases to 66.8%. The partially reversible conversion between poly-SCN and Li_2S indicates a redox process between these two components. However, the reversibility is incomplete; not all Li_2S is fully converted back to poly-SCN after charging. This might be attributed to the fact that we performed XPS analysis on the cathode composite near the current collector/cathode interface where the reaction is incomplete. In addition, the cross-linked −C═N− structure formed during discharge might be coated on the Li_2S particles which would impact reaction kinetics. On the other hand, a slight down-shift of the S 2p peak from 163.1 eV in pristine poly-SCN to 162.8 eV after a discharge/charge cycle is also indicative of polymer chain growth. The elongated polymer chain has more delocalized electrons which would result in a lower binding energy.

Based on these analyses, the discharge/charge mechanism for poly-SCN is proposed in Figure 4G. During discharge, poly-SCN involves the growth of a −C═N− chain and the formation of Li_2S, while after charging, the −C═N− polymer chain reacts with Li_2S to re-form the poly-SCN. Compared to the pristine poly-SCN, the charged poly-SCN has a longer polymer chain.

In summary, we have developed a scalable solid−liquid reaction at room temperature in ambient air to synthesize poly-SCN, a sulfur-rich polymer (55 wt % sulfur). The material has a transition at 77 °C, going from a glassy to a rubbery state. In its rubbery state, the polymer demonstrates high Li^+ conductivity, comparable to the LPSCl ionic conductor at 100 °C. The polymer is applied as an active material in an ASSB which delivers a capacity of 885 mAh g^{-1} at a rate of C/5 at 100 °C. This value is much higher than elemental sulfur (450 mAh g^{-1}) and poly-SCN synthesized by a hand grounding method (480 mAh g^{-1}). Unlike the elemental sulfur cathode which undergoes a "solid−liquid−solid" transition, poly-SCN appears to undergo a single-step solid-state reaction in an ASSB, forming Li_2S along with a polymer with an extended −C═N− chain. After charging, poly-SCN re-forms but with an extended polymer chain length. The high conductivity of poly-SCN in its rubbery state and its excellent thermal stability make it a promising candidate for solid state batteries operating at elevated temperatures. In future studies, further modifications in composition and synthesis processes may enable poly-SCN to serve as a cathode at lower temperatures. These modifications may include refining or reducing the particle sizes, developing improved synthesis procedure to enhance the degree of polymerization, and introducing elemental dopants.

■ ASSOCIATED CONTENT

Supporting Information

The Supporting Information is available free of charge at https://pubs.acs.org/doi/10.1021/acsenergylett.3c00659.

Experimental section, characterizations, detailed discussion of poly-SCN structure reconstruction, and supporting figures (PDF)

Supporting Video S1 for SLR poly-SCN formed from its ionic liquid precursor (MP4)

■ AUTHOR INFORMATION

Corresponding Author

Ping Liu − *Department of Nanoengineering and Materials Science and Engineering Program, University of California San Diego, La Jolla, California 92093, United States;* orcid.org/0000-0002-1488-1668; Email: piliu@ucsd.edu

Authors

Shen Wang − *Department of Nanoengineering, University of California San Diego, La Jolla, California 92093, United States;* orcid.org/0000-0003-3826-4397

Jianbin Zhou − *Department of Nanoengineering, University of California San Diego, La Jolla, California 92093, United States;* orcid.org/0000-0003-0043-9825

https://doi.org/10.1021/acsenergylett.3c00659
ACS Energy Lett. 2023, 8, 2699−2706

Shijie Feng − *Materials Science and Engineering Program, University of California San Diego, La Jolla, California 92093, United States;* orcid.org/0000-0001-5797-8542
Maansi Patel − *Department of Nanoengineering, University of California San Diego, La Jolla, California 92093, United States*
Bingyu Lu − *Department of Nanoengineering, University of California San Diego, La Jolla, California 92093, United States*
Weikang Li − *Department of Nanoengineering, University of California San Diego, La Jolla, California 92093, United States*
Charles Soulen − *Department of Nanoengineering, University of California San Diego, La Jolla, California 92093, United States*
Jiaqi Feng − *Department of Nanoengineering, University of California San Diego, La Jolla, California 92093, United States*
Ying Shirley Meng − *Department of Nanoengineering and Materials Science and Engineering Program, University of California San Diego, La Jolla, California 92093, United States; Pritzker School of Molecular Engineering, University of Chicago, Chicago, Illinois 60637, United States;* orcid.org/0000-0001-8936-8845

Complete contact information is available at: https://pubs.acs.org/10.1021/acsenergylett.3c00659

Author Contributions

‖S.W. and J.Z. contributed equally to this paper.

Notes

The authors declare no competing financial interest.

■ ACKNOWLEDGMENTS

This work was supported by the Advanced Research Projects Agency—Energy, U.S. Department of Energy, under Contract DE-AR0000781. Part of the work used the UCSD-MTI Battery Fabrication Facility and the UCSD—Arbin Battery Testing Facility. TEM, STEM-EDX, and cryo-FIB were performed at the San Diego Nanotechnology Infrastructure (SDNI), a member of the National Nanotechnology Coordinated Infrastructure, which is supported by the National Science Foundation (Grant ECCS-1542148). The use of TGA-DSC, FTIR, and Raman facilities was supported by NSF through the UC San Diego Materials Research Science and Engineering Center (UCSD MRSEC), Grant DMR-201192. We acknowledge the use of facilities and instrumentation at the UC Irvine Materials Research Institute (IMRI), which is supported in part by the National Science Foundation through the UC Irvine Materials Research Science and Engineering Center (Grant DMR-2011967). XPS was performed using instrumentation funded in part by the National Science Foundation Major Research Instrumentation Program under Grant CHE-1338173. We thank the Molecular Mass Spectrometry Facility at UC San Diego for performing the MALDI-TOFMS measurements.

■ REFERENCES

(1) Liu, B.; Fu, K.; Gong, Y.; Yang, C.; Yao, Y.; Wang, Y.; Wang, C.; Kuang, Y.; Pastel, G.; Xie, H.; Wachsman, E. D.; Hu, L. Rapid Thermal Annealing of Cathode-Garnet Interface toward High-Temperature Solid State Batteries. *Nano Lett.* **2017**, *17* (8), 4917−4923.
(2) Lin, X.; Salari, M.; Arava, L. M. R.; Ajayan, P. M.; Grinstaff, M. W. High Temperature Electrical Energy Storage: Advances, Challenges, and Frontiers. *Chem. Soc. Rev.* **2016**, *45* (21), 5848−5887.
(3) Liu, K.; Liu, Y.; Lin, D.; Pei, A.; Cui, Y. Materials for Lithium-Ion Battery Safety. *Sci. Adv.* **2018**, *4* (6), No. eaas9820.
(4) Murugan, R.; Thangadurai, V.; Weppner, W. Fast Lithium Ion Conduction in Garnet-Type Li7La3Zr2O12. *Angew. Chem., Int. Ed.* **2007**, *46* (41), 7778−7781.
(5) Lu, Y.; Huang, X.; Song, Z.; Rui, K.; Wang, Q.; Gu, S.; Yang, J.; Xiu, T.; Badding, M. E.; Wen, Z. Highly Stable Garnet Solid Electrolyte Based Li-S Battery with Modified Anodic and Cathodic Interfaces. *Energy Storage Mater.* **2018**, *15*, 282−290.
(6) Cheng, L.; Chen, W.; Kunz, M.; Persson, K.; Tamura, N.; Chen, G.; Doeff, M. Effect of Surface Microstructure on Electrochemical Performance of Garnet Solid Electrolytes. *ACS Appl. Mater. Interfaces* **2015**, *7* (3), 2073−2081.
(7) Sakuda, A.; Hayashi, A.; Tatsumisago, M. Sulfide Solid Electrolyte with Favorable Mechanical Property for All-Solid-State Lithium Battery. *Sci. Rep* **2013**, *3* (1), 2261.
(8) Haruyama, J.; Sodeyama, K.; Tateyama, Y. Cation Mixing Properties toward Co Diffusion at the LiCoO $_2$ Cathode/Sulfide Electrolyte Interface in a Solid-State Battery. *ACS Appl. Mater. Interfaces* **2017**, *9* (1), 286−292.
(9) Ito, S.; Fujiki, S.; Yamada, T.; Aihara, Y.; Park, Y.; Kim, T. Y.; Baek, S.-W.; Lee, J.-M.; Doo, S.; Machida, N. A Rocking Chair Type All-Solid-State Lithium Ion Battery Adopting Li2O−ZrO2 Coated LiNi0.8-Co0.15Al0.05O2 and a Sulfide Based Electrolyte. *J. Power Sources* **2014**, *248*, 943−950.
(10) Yang, X.; Li, X.; Adair, K.; Zhang, H.; Sun, X. Structural Design of Lithium−Sulfur Batteries: From Fundamental Research to Practical Application. *Electrochemical Energy Reviews* **2018**, *1* (3), 239−293.
(11) Ji, X.; Lee, K. T.; Nazar, L. F. A Highly Ordered Nanostructured Carbon−Sulphur Cathode for Lithium−Sulphur Batteries. *Nat. Mater.* **2009**, *8* (6), 500−506.
(12) Gao, X.; Zheng, X.; Tsao, Y.; Zhang, P.; Xiao, X.; Ye, Y.; Li, J.; Yang, Y.; Xu, R.; Bao, Z.; Cui, Y. All-Solid-State Lithium−Sulfur Batteries Enhanced by Redox Mediators. *J. Am. Chem. Soc.* **2021**, *143* (43), 18188−18195.
(13) Chen, Z.; Liang, Z.; Zhong, H.; Su, Y.; Wang, K.; Yang, Y. Bulk/Interfacial Synergetic Approaches Enable the Stable Anode for High Energy Density All-Solid-State Lithium−Sulfur Batteries. *ACS Energy Lett.* **2022**, *7* (8), 2761−2770.
(14) Pan, H.; Cheng, Z.; He, P.; Zhou, H. A Review of Solid-State Lithium−Sulfur Battery: Ion Transport and Polysulfide Chemistry. *Energy Fuels* **2020**, *34* (10), 11942−11961.
(15) Shim, J.; Striebel, K. A.; Cairns, E. J. The Lithium/Sulfur Rechargeable Cell. *J. Electrochem. Soc.* **2002**, *149* (10), A1321.
(16) Zhang, W.; Zhang, Y.; Peng, L.; Li, S.; Wang, X.; Cheng, S.; Xie, J. Elevating Reactivity and Cyclability of All-Solid-State Lithium-Sulfur Batteries by the Combination of Tellurium-Doping and Surface Coating. *Nano Energy* **2020**, *76*, 105083.
(17) Sun, X.; Li, Q.; Cao, D.; Wang, Y.; Anderson, A.; Zhu, H. High Surface Area N-Doped Carbon Fibers with Accessible Reaction Sites for All-Solid-State Lithium-Sulfur Batteries. *Small* **2022**, *18* (6), 2105678.
(18) Yamamoto, M.; Goto, S.; Tang, R.; Nomura, K.; Hayasaka, Y.; Yoshioka, Y.; Ito, M.; Morooka, M.; Nishihara, H.; Kyotani, T. Nano-Confinement of Insulating Sulfur in the Cathode Composite of All-Solid-State Li−S Batteries Using Flexible Carbon Materials with Large Pore Volumes. *ACS Appl. Mater. Interfaces* **2021**, *13* (32), 38613−38622.
(19) Chen, B.; Deng, S.; Jiang, M.; Wu, M.; Wu, J.; Yao, X. Intimate Triple Phase Interfaces Confined in Two-Dimensional Ordered Mesoporous Carbon towards High-Performance All-Solid-State Lithium-Sulfur Batteries. *Chemical Engineering Journal* **2022**, *448*, 137712.
(20) Sun, Z.; Hu, Y.; Qin, F.; Lv, N.; Li, B.; Jiang, L.; Zhang, Z.; Liu, F. Sulfurized Polyacrylonitrile Cathodes with Electrochemical and Structural Tuning for High Capacity All-Solid-State Lithium−Sulfur Batteries. *Sustain Energy Fuels* **2021**, *5* (21), 5603−5614.
(21) Trevey, J. E.; Gilsdorf, J. R.; Stoldt, C. R.; Lee, S.-H.; Liu, P. Electrochemical Investigation of All-Solid-State Lithium Batteries with

a High Capacity Sulfur-Based Electrode. *J. Electrochem. Soc.* **2012**, *159* (7), A1019−A1022.
(22) Liu, J.; Wang, M.; Xu, N.; Qian, T.; Yan, C. Progress and Perspective of Organosulfur Polymers as Cathode Materials for Advanced Lithium-Sulfur Batteries. *Energy Storage Mater.* **2018**, *15*, 53−64.
(23) Gong, J.; Li, Y.; Zhao, Y.; Wu, X.; Wang, J.; Zhang, G. Metal-Free Polymeric (SCN)n Photocatalyst with Adjustable Bandgap for Efficient Organic Pollutants Degradation and Cr(VI) Reduction under Visible-Light Irradiation. *Chemical Engineering Journal* **2020**, *402*, 126147.
(24) Zhang, Z.; Long, J.; Yang, L.; Chen, W.; Dai, W.; Fu, X.; Wang, X. Organic Semiconductor for Artificial Photosynthesis: Water Splitting into Hydrogen by a Bioinspired $C_3N_3S_3$ Polymer under Visible Light Irradiation. *Chem. Sci.* **2011**, *2* (9), 1826−1830.
(25) Bowman, W. R.; Burchell, C. J.; Kilian, P.; Slawin, A. M. Z.; Wormald, P.; Woollins, J. D. Investigations on Organo−Sulfur−Nitrogen Rings and the Thiocyanogen Polymer, $(SCN)_x$. *Chem.—Eur. J.* **2006**, *12* (24), 6366−6381.
(26) Kerridge, D. H.; Mosley, M. Parathiocyanogen [(SCN) x]: A Novel Chemical Oxidation Product of Molten Potassium Thiocyanate. *Journal of the Chemical Society D: Chemical Communications* **1969**, *9*, 429.
(27) Krishnan, P.; Advani, S. G.; Prasad, A. K. Synthesis and Evaluation of Polythiocyanogen (SCN)x as a Rechargeable Lithium-Ion Battery Electrode Material. *J. Power Sources* **2011**, *196* (18), 7755−7759.
(28) Kahani, S. A.; Sabeti, M. The Mechanochemical Oxidation of Thiocyanate to Polythiocyanogen (SCN) n Using Peroxydisulphate. *J. Inorg. Organomet Polym. Mater.* **2011**, *21* (3), 458−464.
(29) Wilson, I. R.; Harris, G. M. The Oxidation of Thiocyanate Ion by Hydrogen Peroxide. II. The Acid-Catalyzed Reaction. *J. Am. Chem. Soc.* **1961**, *83* (2), 286−289.
(30) Zhang, S. Understanding of Sulfurized Polyacrylonitrile for Superior Performance Lithium/Sulfur Battery. *Energies (Basel)* **2014**, *7* (7), 4588−4600.
(31) Lee, Y.-G.; Fujiki, S.; Jung, C.; Suzuki, N.; Yashiro, N.; Omoda, R.; Ko, D.-S.; Shiratsuchi, T.; Sugimoto, T.; Ryu, S.; Ku, J. H.; Watanabe, T.; Park, Y.; Aihara, Y.; Im, D.; Han, I. T. High-Energy Long-Cycling All-Solid-State Lithium Metal Batteries Enabled by Silver−Carbon Composite Anodes. *Nat. Energy* **2020**, *5* (4), 299−308.
(32) Fang, R.; Xu, H.; Xu, B.; Li, X.; Li, Y.; Goodenough, J. B. Reaction Mechanism Optimization of Solid-State Li−S Batteries with a PEO-Based Electrolyte. *Adv. Funct Mater.* **2021**, *31* (2), 2001812−2001818.
(33) Yu, T.; Li, F.; Liu, C.; Zhang, S.; Xu, H.; Yang, G. Understanding the Role of Lithium Sulfide Clusters in Lithium−Sulfur Batteries. *J. Mater. Chem. A Mater.* **2017**, *5* (19), 9293−9298.
(34) Park, S. W.; Oh, G.; Park, J.; Ha, Y.; Lee, S.; Yoon, S. Y.; Kim, B. G. Graphitic Hollow Nanocarbon as a Promising Conducting Agent for Solid-State Lithium Batteries. *Small* **2019**, *15* (18), 1900235.

https://doi.org/10.1021/acsenergylett.3c00659
ACS Energy Lett. 2023, 8, 2699−2706